Enhanced ultrasound transmission through the human skull using shear mode conversion

G. T. Clement, P. J. White, and K. Hynynen
Department of Radiology, Harvard Medical School, Brigham and Women's Hospital, Boston, Massachusetts 02145

(Received 22 August 2003; revised 2 December 2003; accepted 15 December 2003)

A new transskull propagation technique, which deliberately induces a shear mode in the skull bone, is investigated. Incident waves beyond Snell's critical angle experience a mode conversion from an incident longitudinal wave into a shear wave in the bone layers and then back to a longitudinal wave in the brain. The skull's shear speed provides a better impedance match, less refraction, and less phase alteration than its longitudinal counterpart. Therefore, the idea of utilizing a shear wave for focusing ultrasound in the brain is examined. Demonstrations of the phenomena, and numerical predictions are first studied with plastic phantoms and then using an *ex vivo* human skull. It is shown that at a frequency of 0.74 MHz the transskull shear method produces an amplitude on the order of—and sometimes higher than—longitudinal propagation. Furthermore, since the shear wave experiences a reduced overall phase shift, this indicates that it is plausible for an existing noninvasive transskull focusing method [Clement, Phys. Med. Biol. **47**(8), 1219–1236 (2002)] to be simplified and extended to a larger region in the brain. © *2004 Acoustical Society of America.*
[DOI: 10.1121/1.1645610]

PACS numbers: 43.80.Sh, 43.20.El [FD] Pages: 1356–1364

I. INTRODUCTION

Coherent noninvasive focusing of ultrasound through the human skull has been suggested for a number of therapeutic and diagnostic implications in the brain. For example, ultrasound has been considered as a tool for the transskull treatment of brain tumors,[1–3] targeted drug delivery, improved thrombolytic stroke treatment,[4] blood flow imaging,[5,6] detecting internal bleeding,[7] and tomographic brain imaging.[8–12] Although the human skull has been the barrier to the clinical realization of many of these applications, recent studies have demonstrated both minimally invasive and noninvasive aberration correction methods for transskull focusing. Minimally invasive approaches use receiving probes designed for catheter insertion into the brain[13,14] to measure the amplitude and phase distortion caused by the skull, and then use this information to correct the beam using an array.[15] Alternatively, a completely noninvasive approach uses x-ray computed tomography (CT) images to predict the longitudinal wave distortion caused by the skull.[16] Noninvasive focusing with a therapeutic array has been demonstrated with a longitudinal wave propagation model, but the amplitude of the focus was observed to drop when the focus was directed close to the skull surface.

The assumption that the transcranial propagation is composed of purely longitudinal modes is valid for small incident beam angles,[17] but this assumption rapidly breaks down beyond approximately 25°, as the longitudinal wave approaches its critical angle. This is a plausible explanation for the reduced amplitude observed using the longitudinal model; as the focus was directed toward the periphery of the brain, an increasing number of array elements were oriented at higher incident angles to the skull.

Modeling of shear waves in previous work had been dismissed as being either of insignificant amplitude,[17] or (if significant) as inoperative since the resulting beam would be distorted and hard to predict.[18] The absence of significant information on the skull bone's elastic wave speeds also has prohibited its consideration in modeling. However, a complex conversion from a longitudinal wave (skin) to a shear wave (skull) and back to a longitudinal wave (brain) does not necessarily produce a highly distorted or small-amplitude wave. Our present experimental and theoretical investigations with isotropic phantom materials and an *ex vivo* human skull bone support this hypothesis. In fact, we show that a focused beam traveling as a shear wave in the skull may be less distorted than a longitudinal one. In some instances a focused beam is actually observed to be larger in amplitude than a longitudinal wave propagated through the same skull area. The success of the longitudinal-shear-longitudinal propagation is primarily due to the similarities between the elastic (shear) wave speed ($\sim$1400 m/s) and the sound speeds of water ($\sim$1500 m/s), skin ($\sim$1525 m/s), and the brain ($\sim$1550 m/s). In contrast, the range of longitudinal sound speeds in the skull at relevant frequencies is approximately twice these values.

On the basis of these properties, we examine the possibility of intentionally producing shear modes in the skull bone as a mechanism for producing or enhancing a focus through the skull. We incorporate shear modes into a previously described transskull propagation model, demonstrating a significantly improved ability to predict ultrasound phase and amplitude at high incident angles. To illustrate the approach, we first model the field through a single plastic layer. The approach is then applied to sections of human bone, which are compared to experimental measurements. The approach could be used for more accurate focusing in the brain and could extend the focusing region beyond current methods.

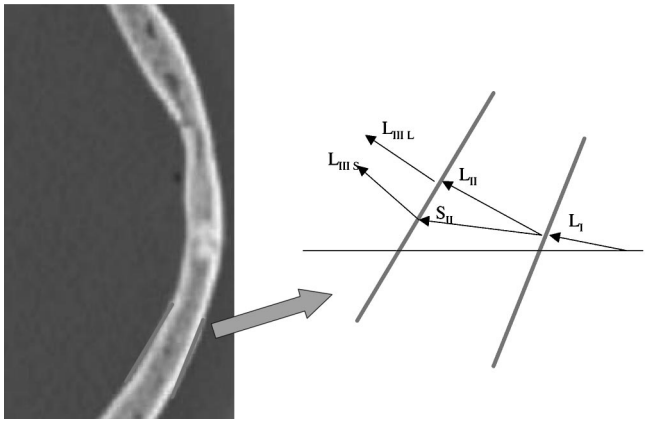

FIG. 1. CT images (left) are segmented in to areas consisting of three-dimensional nonparallel plates. The model then considers isotropic propagation within the bone.

II. TRANSSKULL SHEAR MODE PROPAGATION

Based on the skull's small curvature relative to ultrasound wavelengths,[17,19] the inner and outer surfaces of the skull are sectioned into regions that are each approximated as flat, but not necessarily parallel. A diagram of the problem is given in Fig. 1, showing the one region of the ultrasound field incident upon skull surface. Each region is then modeled as a single-layer isotropic solid with Lamé constants determined as a function of the mean density over the propagation region.

Propagation through an arbitrarily oriented isotropic skull layer is achieved by spectral decomposition of the incident wave, followed by the determination of the ray paths, and attenuation as a function of angular wave number as the field crosses the skull. Each of these initially longitudinal harmonic spectral wave components will be considered below in terms of its velocity potential. Without loss of generalization, a given component may be viewed in a reference frame where the surface normal is oriented along the Cartesian y axis, with the z axis defined by the unit vector of the cross product between the propagation axis and the surface vector. In this frame, the velocity potential is expressed as

$$\phi^I = A_L^I e^{i(\omega t - k_x^I x \sin\theta^I - k_y^I y \cos\theta^I)} + A_{LR}^I e^{i(\omega t - k_x^I x \sin\theta^I + k_y^I y \cos\theta^I)}, \tag{1}$$

where A_L is the amplitude of the longitudinal wave component incident upon the layer surface, A_{LR} is the amplitude of the reflected longitudinal wave, θ is the angle of incidence, and k_x and k_y are the wave vector components in the specified reference frame. The superscripts I to III are used to denote the skin, skull, and brain, respectively, while the subscripts L and S refer to longitudinal or shear waves. Accordingly, the transmitted longitudinal potential in the skull is given by

$$\phi^{II} = A_L^{II} e^{i(\omega t - k_x^{II} x \sin\theta^{II} - k_y^{II} y \cos\theta^{II})}, \tag{2}$$

and the shear vector potential is

$$\boldsymbol{\psi}^{II} = A_S^{II} e^{i(\omega t - k_{S_x}^{II} x \sin\theta_S^{II} - k_{S_y}^{II} y \cos\theta_S^{II})} \hat{z}. \tag{3}$$

Using this description, each spectral wave component must be viewed in its own unique reference frame. At the boundary, the incident wave is split into a reflected wave, a transmitted longitudinal wave, and a transmitted shear wave. The amplitudes of these waves may be determined relative to the incident wave using methods outlined by Kino.[20] Specifically, the normal component of the particle displacement

$$\mathbf{r} = \nabla\phi + \nabla\times\boldsymbol{\psi}, \tag{4}$$

must be continuous at the boundary as well as the normal stress

$$S_{yy} = \lambda \frac{\partial r_x}{\partial x} + (\lambda + 2\mu)\frac{\partial r_y}{\partial y}, \tag{5}$$

and the shear stress

$$S_{xy} = \mu\left(\frac{\partial r_x}{\partial y} + \frac{\partial r_y}{\partial x}\right), \tag{6}$$

with the shear and longitudinal sound speed of a given medium related to the Lamé constants μ and λ by

$$c_S = \sqrt{\frac{\mu}{\rho}}, \quad c_L = \sqrt{\frac{\lambda + 2\mu}{\rho}}. \tag{7}$$

Details of the amplitude calculations are provided in Appendix A. It is stressed that each plane-wave solution describes the behavior of only a single angular wave number. It is necessary to calculate these amplitudes for each component wave vector space. However, this may be readily performed in closed form, as given in Appendix B.

After propagating into the skull, the longitudinal and shear waves are treated separately, with the total wave reaching the brain then equal to

$$\phi^{III} = A_{LL}^{III} e^{i(\omega t - k_x^{III} x \sin\theta^{III} - k_y^{III} y \cos\theta^{III})} + A_{LS}^{III} e^{i(\omega t - k_x^{III} x \sin\theta_S^{III} - k_y^{III} y \cos\theta_S^{III})}, \tag{8}$$

where A_{LL}^{III} and A_{LS}^{III} are the amplitudes of the longitudinal waves due to the incident longitudinal and shear waves in the skull, respectively. The values of the velocity potentials may be found by equating Eqs. (4) through (6) at the skin–bone interfaces after substituting in Eqs. (1) to (3), and solving for A_L^{II} and A_S^{II}. At the skull–brain interface, the incident shear and longitudinal velocity potential amplitudes will be equal to the product of these transmission amplitudes and the absorption loss experienced within the bone. Since each spectral component will have its own independent path length through the skull, its total absorption will generally differ between components. A two-dimensional representation of the problem is given in Fig. 1.

To find the wave amplitudes in the brain, A_{LL}^{III} and A_{LS}^{III}, the problem is once again reduced to two dimensions by rotating the problem into a reference frame where the surface normal is oriented along the Cartesian y axis and the relevant wave vector lies in the $x-y$ plane. Since the soft tissue of the brain is fluid-like, the incident longitudinal wave in the skull bone will be further divided into a reflected shear wave, a reflected longitudinal wave, and a transmitted longitudinal

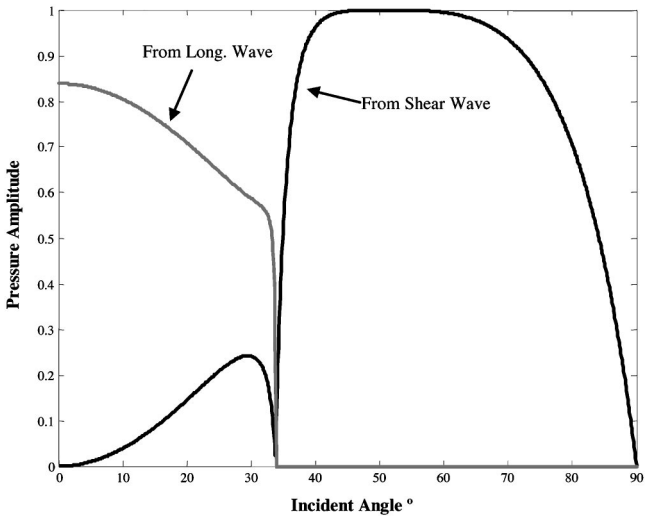

FIG. 2. Calculated pressure amplitude of a planar wave after liquid–solid (Plexiglas)–liquid propagation.

wave. The shear wave in the skull will be similarly divided, but with differing reflection and transmission angles.

The acoustic pressure at a given point in the brain is obtained by separately solving for the amplitude and phase of each spectral component over a planar area. The spectrum is then inverse transformed to give the pressure over the measurement plane. The pressure amplitude is equal to the negative of the normal stress which is related to the amplitude of the scalar velocity potentials in the brain, A_{LL}^{III} and A_{LS}^{III}, by Eq. (4) and Eq. (5). Figure 2 shows the angular dependence of A_{LL}^{III} and A_{LS}^{III} resulting from an infinite plane wave in water after traveling through an ideal acrylic layer. A similar plane-wave methodology was examined by Thompson[21] for examining Doppler beams through plastic.

Based on the skull's high attenuation coefficient,[18] we neglect additional contributions due to multiple reflections within the skull bone.[18,22] The total acoustic pressure at any point in the brain can be determined by calculating the path length and total transmission amplitude for each spectral component. These values then allow the relative acoustic phase and the overall attenuation (including absorption loss) to be estimated. The algorithm for determining the field path lengths from the transducer to the measurement point in the brain is presented in Appendix B. A special case of the method was previously used to trace the longitudinal path length of elements from an array in order to focus ultrasound through human skulls.[16] In that study, sections of the inner and outer surfaces of the skull were assumed to be parallel and shear waves were neglected.

III. PROPAGATION ALGORITHM

We first consider a parallel plastic plate to test the algorithm in order to provide an idealized isotropic case readily verifiable by experiment. The identical plate was previously used in a study involving the propagation of longitudinal waves from a planar source at small incident angles.[23] Relevant values for the plastic are summarized in Table I. The ultrasound source is a 1.5-MHz focused transducer with a diameter of 120 mm and a radius of curvature equal to 160 mm. The source function for the algorithm is acquired by projecting a laboratory-measured pressure field from a plane near the geometric focus backward to the source.[24] This field is measured over a 30×30-mm^2 area with a spatial resolution of 0.5 mm. The source function is then propagated through the plates using an algorithm described numerically in Appendixes A and B. The distance from the source to the measured plane is 121 mm and that from the plastic inner surface to the source is 61 mm.

Similar methodology is used to propagate through *ex vivo* human calvaria (brain cages). Following the laboratory measurements, water is used as the interfacing medium between both the inner and outer skull surface. The ultrasound source for the transskull measurement is a 0.74-MHz focused transducer with a diameter of 8 cm and a radius of curvature equal to 150 mm.

The numeric algorithm is implemented in MATLAB, using matrix-based operations for the layers. Operations were performed on a 1-GHz AMD-based PC. A typical projection of a complex 128×128 matrix through five layers took approximately 30 s to calculate.

IV. EXPERIMENT

A. Skull registration and density

Data for the simulation were obtained from a digitized human-head profile obtained using CT images (Siemens, SOMATOM, AH82 Bone Kernel). Both the coordinates of the skull surfaces as well as the internal density variation were obtained from these images. Scans were taken at 1-mm intervals using a 200×200-mm field of view. A polycarbonate stereotaxic frame was attached around each sample to allow the skulls to be attached to the array and provide a reference for the mechanical positioning system and the CT images. The calculation was performed only in bone lying within the beamwidth of the section being considered. Information about the shape and structure of an individual calvarium was acquired by combining the images, which returned intensities proportional to material density. In the present demon-

TABLE I. Summary of materials and their acoustic properties, including density, longitudinal absorption coefficient, shear absorption coefficient, longitudinal and shear sound speeds, and thickness across the axis of propagation.

Material	Density (kg/m^3)	a_L (Np/m)	a_S (Np/m)	C_L (m/s)	C_S (m/s)	Thickness (mm)
Plastic	1187	45	50	2185	1330	11.8
Skull	2186	85	90	2850	1400	5.29
Water	1000	0	0	1486	NA	Variable

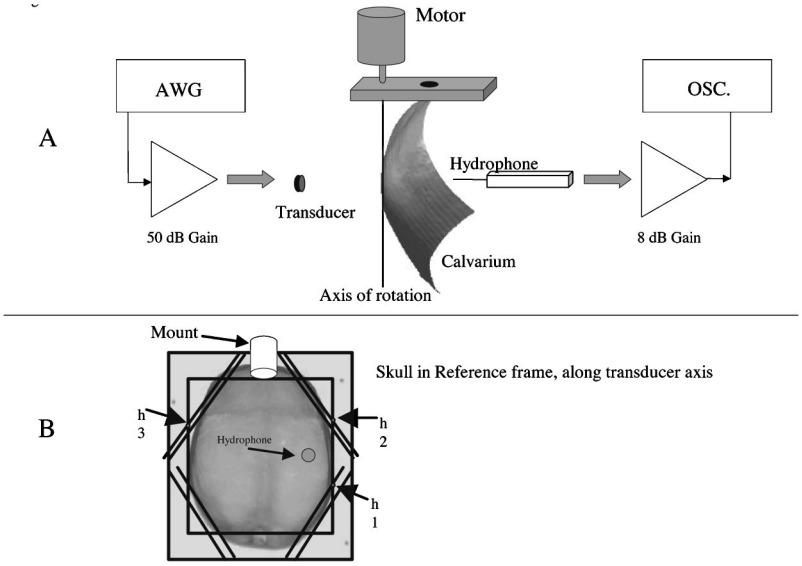

FIG. 3. (A) The experimental setup. (B) An overhead view showing the relative position of the hydrophone within the skull specimen.

stration, the mean density across the layer was used, effectively approximating the skull as an isotropic solid.

Coordinates of points along the inner and outer surfaces of the skull were identified on an image using a threshold filter, which searched for the innermost and outermost densities $>1.4\ \mathrm{gm/cm^3}$ along each line of an image. Points of successive images were combined to give three-dimensional representation of the inner and outer skull surface. Pixel intensities of each image were also combined into a three-dimensional array for later processing.

The projection algorithm relied on precise knowledge of the orientation of the skull relative to individual array elements. To achieve this, the phasing algorithm translated and rotated the skull data from the CT coordinate frame to the transducer coordinate frame as well as translated and rotated the skull from the mechanical positioning system's coordinate frame to the transducer coordinate frame. The program operated using three markers located on the polycarbonate frame affixed to the skull. These locations could be identified mechanically with the positioning system to a precision of approximately 0.1 mm. The algorithm then generated a rotation matrix that mapped between the coordinate systems.

B. Ultrasound measurements

Propagation experiments were set up in a water tank to verify the numeric algorithm. Measurements were performed in degassed and deionized water in a tank padded with rubber to inhibit reflections. Ultrasound signals were generated by a transducer specific to the particular measurement and received with a polyvinylidene difluoride (PVDF) needle hydrophone (Precision Acoustics, Dorchester, UK). To assure a strong reception while maintaining accuracy, a 0.2-mm-diameter hydrophone was used for the 1.5-MHz measurements and a 0.5-mm-diameter hydrophone was used for measurements at 0.74 MHz. The smaller hydrophone at higher frequency was used to minimize hydrophone directivity and prevent phase averaging. A skull (or plastic plate) was placed between the hydrophone and transducer at an angle controlled by a rotational stepping motor (Velmex, New York). A 3D linear positioning system (Velmex, model V P9000) allowed the hydrophone to be scanned over a measurement area centered about the transducer's axis of symmetry. Transducer signals were generated by an arbitrary waveform generator (Wavetek, California, model 305) fed to a power amplifier (ENI, New York, model 2100L). The hydrophone's voltage response was sent though a Precision Acoustics preamp and an amplifier (Preamble Instruments, Oregon, model 1820) before it was recorded by a digital oscilloscope (Tektronix, Oregon, model 380). The voltage waveform was downloaded to a PC by GPIB control and the amplitude and phase at the measurement location were calculated from the FFT of the signal, taking the values at the transducer driving frequency.

The 11.8-mm plastic plate was placed in the test tank and the acoustic transmission was measured on the transducer's axis of symmetry, 121 mm from its face. The acoustic pressure was measured between $-70°$ and $70°$ at an increment of $1°$. Agreement between the measured and simulated waveforms was evaluated by comparing the amplitudes and phases at each angular orientation. The source function for the simulation was a pressure field measurement taken with the transducer in water without a plate present.

For the transskull measurements, two different mounting procedures were performed. The first, shown in Fig. 3(a), was designed to allow measurement through an approximately constant location on the skull at different incident angles. The second configuration, Fig. 3(b), allowed measurement at high incident angles with good registration between the transducer and the skull, but did not facilitate movement of the skull. Initial measurements examined the angular dependence of amplitude on the skull, in order to determine whether amplitude peaks were present beyond the longitudinal Snell's critical angle. A section of skull bone was rotated between $0°$ and $55°$, with the axis of rotation normal to the transducer axis and coincident with a line through the bone. The maximum angle of $55°$ was the highest value obtainable with the current setup.

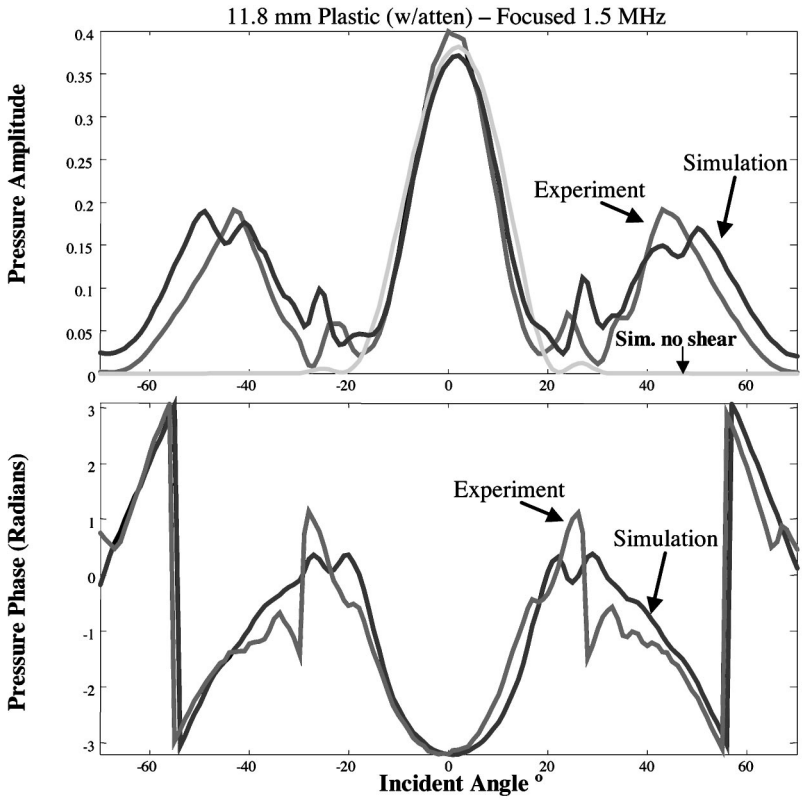

FIG. 4. The on-axis amplitude and phase simulated (dashed), simulated without a shear mode (solid), and measured (dotted) after propagation through an 11.8-mm plastic plate with a focused 1.5-MHz beam.

V. RESULTS

A. Plastic

The correlation between the measured and predicted fields is shown in Fig. 4. For reference, the plot also includes the amplitude of the numeric calculation obtained when shear waves were neglected. The amplitudes and phases of all three curves match closely for incident angles with absolute values below 31°, which is the longitudinal critical angle for the signal's spectral peak. However, beyond this angle, the longitudinal-only simulation is unable to predict the second local maximum in the amplitude, which results from a purely elastic wave within the sample. The major source of discrepancy between the measured data and simulated amplitude possibly results from underestimation of the shear wave absorption coefficient in the simulations. This effect becomes more pronounced at high angles, where the path length is largest. However, very good correlation is found between the simulated and measured ultrasound phase. This agreement extended to nearly all angles, with the exception of the transitional region between 20° and 30°, the region where the wave amplitude is near its minimum. Neglecting this region, 76% of the remaining calculated points deviated from measurements by $\pi/6$—or less—radians.

B. Transskull measurement

By rotating the skull, a local pressure transmission maximum was observed at 32°. This signal is expected to result almost entirely from shear propagation through the bone, based on a longitudinal critical angle of about 30°. Further evidence of the wave's origin as a shear wave at higher incident angles is found in the measured data (Fig. 5), which

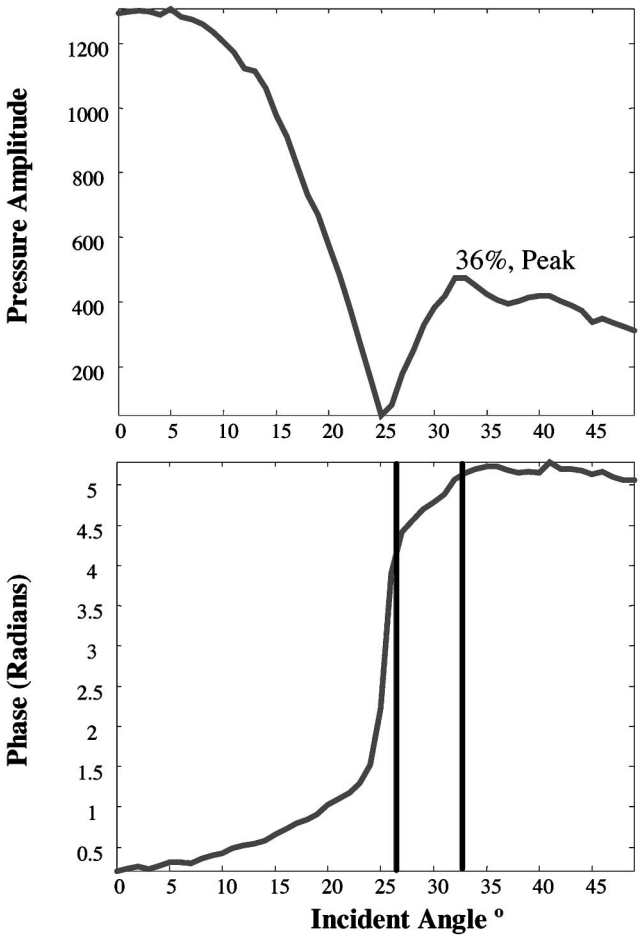

FIG. 5. The on-axis amplitude and phase measured after propagation through a skull bone. The black lines indicate the transition in phase to an entirely shear mode.

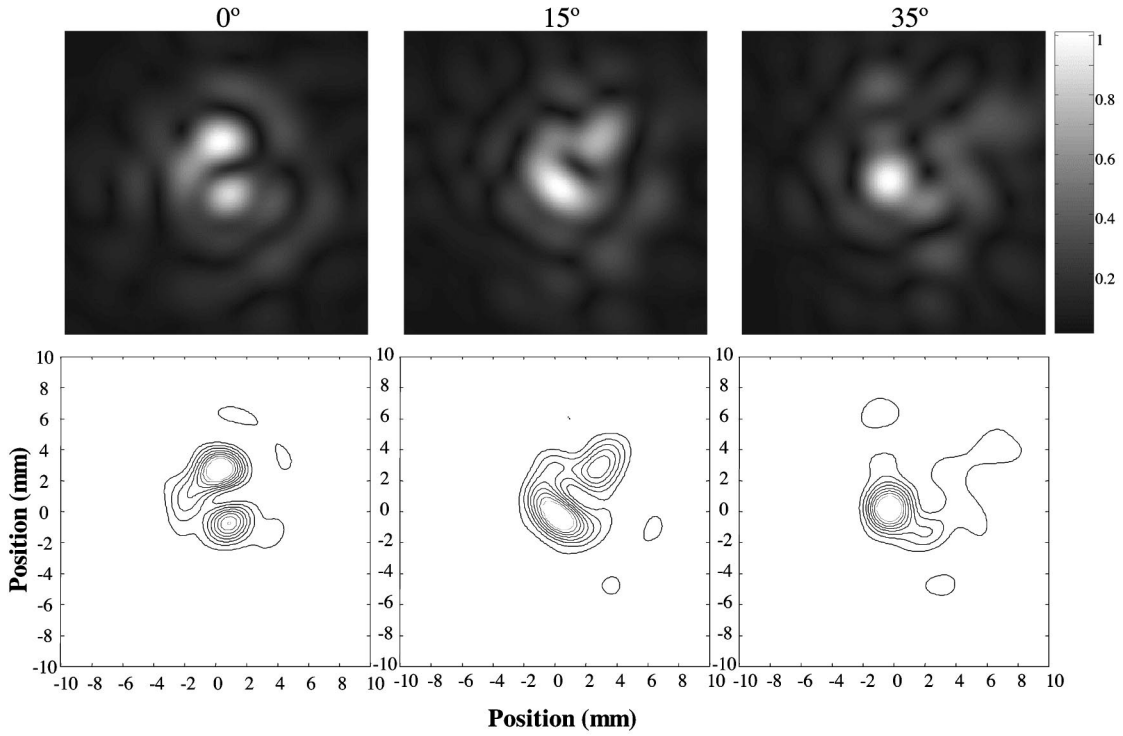

FIG. 6. Transskull ultrasound signal measured at 0°, 15°, and 35° incidence. The measurement indicates reduced distortion beyond Snell's critical angle for the longitudinal mode.

shows the angular dependence of the wave phase. Below 26° the phase closely resembles the behavior of a purely longitudinal wave. Between 26° and 32° there is a deceleration in the slope, indicating a region of superimposed contribution from the shear and longitudinal wave. Beyond 32° the slope is approximately linear and negative, since the shear sound speed is less than the speed of sound in water.

Using the same mounting configuration, field measurements were performed over a 30×30-mm area with 1-mm resolution for different incident angles. Figure 6 shows the field immediately after passing through the skull bone after measurements at 0°, 15°, and 30°, showing less distortion in the signal propagated through the skull as a shear wave than when propagated in a longitudinal mode at both 0° and 15°.

A second set of measurements was performed with skulls placed in reference frames for spatial correlation with CT images. Although only an estimated value of the shear wave speed was used for the study, accurate spatial registration and data for the longitudinal modes allowed the longitudinal critical angle to be identified. Skulls were then aligned to assure that the transmitted signal was from shear propagation in the bone.

Finally, a demonstration was performed with a skull placed in a reference frame, to allow spatial correlation with CT images. Accurate spatial registration and data for the longitudinal modes allowed the longitudinal critical angle to be identified. However, only an estimated value of the shear wave speed was available for the study.[17] Skulls were aligned to assure that the transmitted signal was from shear propagation in the bone. Figure 7 shows a line measurement of the field, with the outer surface of the skull oriented at 32° relative to the axis of symmetry. Although there is discrepancy between the simulation and the measurement, the simulation was nonetheless able to identify the presence of the focused shear wave, with a beam shape resembling that of the measurement.

VI. DISCUSSION

Our preliminary simulations and experimental measurements indicate that transmission of a coherent, focused ultrasound beam through the skull purely as a shear wave is possible. At the presently considered driving frequency near 0.7 MHz, the peak amplitude through the skull due to shear propagation in the bone was found to be between 35% and 55% of the peak longitudinal mode. Although the shear amplitude was lower than longitudinal modes, we found evidence that the overall beam may suffer less distortion when propagated through a localized region of the bone. Furthermore, the shear mode experienced less phase distortion due to the similarity between the shear wave speed and the speed of sound in water. Comparable similarities could be found in soft tissues.

More precise correlation between the simulation and measured data will require accurate measurement of the shear wave speed in the skull bone. The present study used a previously tabulated value of 1400 m/s.[17] It is likely, however, that this value fluctuates as a function of position on the skull and could potentially be correlated either with bone density and/or with bone type (cortical or trabecular).

There are several possible direct implications of the shear transmission method: First, the method may be added to pre-existing noninvasive transskull phasing algorithms for

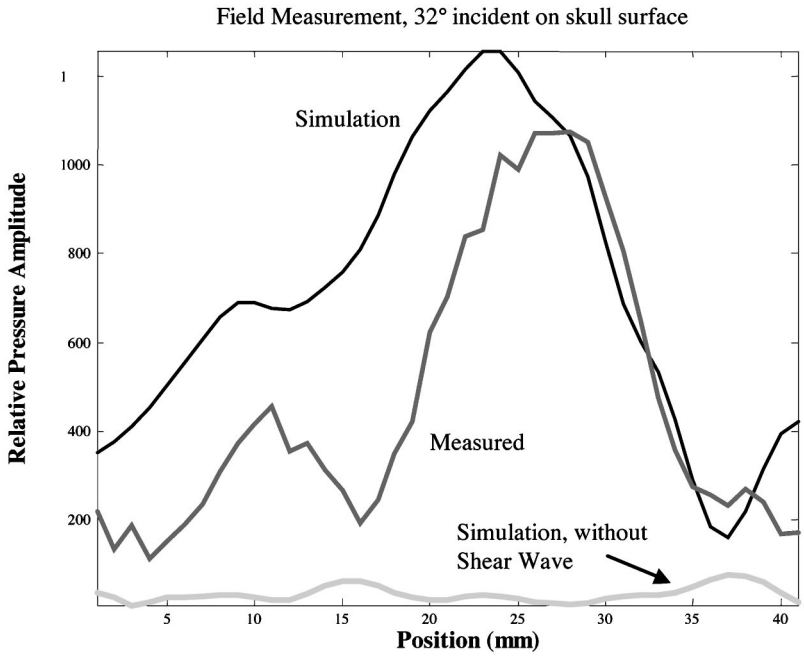

FIG. 7. A linear hydrophone measurement of a transskull ultrasound beam (solid). The measurement is taken parallel to the transducer's propagation axis and passes through the transducer's geometric focus. This scan is compared to a model with (dashed) and without (dotted) consideration of shear propagation in the skull.

improved focusing at high incident angles. This is particularly important when focusing close to the skull surface, where high angular incidence is necessary. Second, the method may have application in transskull imaging, where a narrow ultrasound beam would be directed through the skull and intentionally high incident angles. Finally, the method could potentially be used to detect flow in the brain by means of frequency Doppler shifts. All of these techniques are expected to be feasible in the submegahertz frequency range considered here.

ACKNOWLEDGMENTS

This work was supported by Grants 9R01EB003268 and R21EB00705 from the National Institutes of Health.

APPENDIX A: TRANSMISSION AMPLITUDES

The pressure amplitudes were calculated by solving for the velocity potentials described in Eqs. (1), (2), (3), and (8). After linear algebraic simultaneous solution of the equations, it may be shown that the shear and longitudinal wave amplitudes in the bone are given by

$$A_S^{II}(\theta^I)=\frac{-4A_L^I c^{I^2}k^{I^2}k_L^{II}\rho^I\cos\theta^I\cos\theta_L^{II}\sin\theta_L^{II}/k_S^{II}}{D_{II}(\theta^I)\rho^{II}\cos\theta^I+c_{II}^2k^I\rho^{II}C_{II}(\theta^I)}, \tag{A1}$$

and

$$A_L^{II}(\theta^I)=\frac{2A_L^I c^{II^2}k^{I^2}k_S^{II}\rho^I\cos\theta^I\cos 2\theta_S^{II}/k_L^{II}}{D_{II}(\theta^I)\rho^{II}\cos\theta^I+c^{II^2}k^I\rho^I\cos\theta_L B_{II}(\theta^I)}, \tag{A2}$$

where

$$B_{II}(\theta^I)=k_S^{II}\cos 2\theta_S^{II}+2k_L^{II}\sin\theta_L^{II}\sin\theta_S^{II}, \tag{A3}$$

$$C_{II}(\theta^I)=k_S\cos\theta_L^{II}\cos 2\theta_S^{II}+k_L\sin 2\theta_S^{II}\sin\theta_S^{II}, \tag{A4}$$

$$D_{II}(\theta^I)=k_L^{II}k_S^{II}(c_L^{II^2}\cos 2\theta_S^{II}-2c_S^{II^2}\sin\theta_L^{II}\times\sin(\theta_L^{II}-2\theta_S^{II})), \tag{A5}$$

and the transmitted angles are understood to be functions of θ, related by Snell's law

$$\frac{\sin\theta^I}{c^I}=\frac{\sin\theta_L^{II}}{c_L^{II}}=\frac{\sin\theta_S^{II}}{c_S^{II}}. \tag{A6}$$

The amplitudes of the waves transmitted into the brain from the incident longitudinal and shear waves are equal to

$$A_{LS}^{III}(\theta^I)=\frac{-(2A_S^{II}(\theta^I)c_S^2k_S^2\rho_{sk}\cos\theta_L^{II'}(k_S\cos 2\theta_S^{II'}+2k_L\sin\theta_S^{II'})\sin 2\theta_S^{II'})/k^{III}}{D(\theta^I)\rho^{II}\cos\theta^{III}+c^{III^2}k^{III}\rho^{III}C_{II}(\theta^I)} \tag{A7}$$

and

$$A_{LL}^{III}(\theta^I)=\frac{2A_L^{II}(\theta^I)k_L^{II^2}\rho^{II}\cos\theta_L(c_L^{II^2}-c_S^{II^2}+c_S^{II^2}\cos 2\theta_L^{II})B_{II}(\theta^I)/k^{III}}{\rho^{II}\cos\theta^{III}D_{II}(\theta^I)+c^{III^2}k^{III}\rho^{III}\cos\theta_L^{II}B_{II}(\theta^I)}. \tag{A8}$$

APPENDIX B: PROPAGATION ALGORITHM

Regardless of whether or not the layers are parallel, the transfer function through the layers may still be written in a closed form in terms of the thickness across the z axis, z_n, the sound speed c_n, and density of each layer ($n=I$, II, III). For each interface it is necessary that the unit vectors normal to the layer surfaces $\hat{n}_n$ be calculated. For a given initial wave vector $\mathbf{k}_{0xy}$, the ray path from (0,0, z_0) between any two surface interfaces traverses a distance of

$$|\mathbf{R}_{nxy}| = \frac{(\mathbf{z}_{nxy} - \mathbf{r}_{nxy}) \cdot \hat{n}_{n+1}}{\hat{k}_{nxy} \cdot \hat{n}_{n+1}}, \tag{B1}$$

where, as depicted in Fig. 1, $\mathbf{r}_{nxy}$ is the vector extending along the layer from z axis to the intercept of the layer with the ray. The unit vector along the wave vector's path is given by $\hat{k}_{nxy}$. Again, the frequency dependence on the wave vector orientation is understood. It follows that the ray position vector must be equal to $\mathbf{R}_{nxy} = |\mathbf{R}_{nxy}| \hat{k}_{nxy}$. Although the initial wave vector orientation, $\hat{k}_{0xy}$, is known, the direction of the wave vector in the first and subsequent layers must be calculated using the relation[25]

$$\frac{1}{c_n}(\hat{n}_{n+1} \times \hat{k}_{nxy}) = \frac{1}{c_{n+1}}(\hat{n}_{n+1} \times \hat{k}_{n+1xy}), \tag{B2}$$

which is a consequence of Snell's law in three-dimensional space that requires the incident wave vector, the transmitted wave vector, and the normal vector all be in the same plane. After bifurcation of the wave into a longitudinal and shear mode, the waves are treated separately. The transmitted wave vector on the right-hand side of Eq. (B2) may be obtained by crossing both sides of the equation with $\hat{n}_{n+1}$. Using cross-product relations, it may be shown that

$$\hat{k}_{n+1xy} = \frac{c_{n+1}}{c_n}(\hat{k}_{nxy} - \cos \gamma_{i_{n+1xy}} \hat{n}_{n+1}) + \cos \gamma_{i_{n+1xy}} \hat{n}_{n+1}. \tag{B3}$$

The incident unit wave vector of the nth layer is simply equal to the transmitted wave of the $(n-1)$st layer. With the exception of the 0th layer shown in Fig. 2, it is also necessary to find $\mathbf{r}_{nxy}$ in order to calculate Eq. (B1). Given the thickness across the z axis of each layer, the point of intersection of ray $\mathbf{R}_n$ with the surface of the $n+1$ layer is

$$\mathbf{r}_{n+1} = \mathbf{R}_n + \mathbf{r}_n - \mathbf{z}_n. \tag{B4}$$

Over a series of N layers, the phase of a ray reaching the Nth plane $\phi_R(\mathbf{k}_{Nxy}, \omega)$ is the sum of the phase contributions over each path length given by Eq. (B1). The *spatial* phase at the plane z, is related to the ray phase at N by $\phi_N(\mathbf{k}_{Nxy}, \omega) = \phi_R(\mathbf{k}_{Nxy}, \omega) - 2\pi k_N r_N \sin \gamma_{Nxy}$, as illustrated in Fig. 1. A ray leaving the initial plane with a polar angle $\gamma_{0xy}(\omega)$ will arrive at the plane z with a new orientation $\gamma_{Nxy}(\omega)$ determined by the $N-1$ unit vector $\hat{k}_{N-1}$

$$\phi(\mathbf{k}_{Nxy}, \omega, z) = \phi(\mathbf{k}_{0xy}, \omega, z_0) + \sum_{n=0}^{N-1} k_n \frac{(\mathbf{z}_n - \mathbf{r}_n) \cdot \hat{n}_{n+1}}{\hat{k}_n \cdot \hat{n}_{n+1}} - \sin \gamma_{Nxy}(\omega), \tag{B5}$$

given $\phi(\mathbf{k}_{0xy}, \omega, z_0)$, the phase of $\tilde{p}(k_x, k_y, \omega, z_0)$ at the initial plane.

The pressure over the plane at z can be expressed in terms of the ray phase presented in Eq. (B5) and the transmission coefficient by

$$\tilde{p}(\mathbf{k}_{Nxy}, \omega, z) = \tilde{p}(\mathbf{k}_{0xy}, \omega, z_0) e^{-i \sin \gamma_{Nxy}(\omega)} \times \left[\prod_{n=1}^{N-1} T_{nxy}(\omega) e^{i \phi_N(\mathbf{k}_{Nxy}, \omega, z)} \right], \tag{B6}$$

where the terms in square brackets on the right-hand side of Eq. (B6) can be viewed as an operator that maps the field from k_0 space to a new k_N space. In the present problem, the amplitudes, T, are given by to Eqs. (A7) and (A8) and the component angles, γ_{Nxy}. In practice, this mapping requires interpolation to produce a linearly spaced matrix at z.

[1] F. J. Fry, "Transkull transmission of an intense focused ultrasonic beam," Ultrasound Med. Biol. **3**(2–3), 179–184 (1977).
[2] J. Tobias, K. Hynynen, R. Roemer, A. N. Guthkelch, A. S. Fleischer, and J. Shively, "An ultrasound window to perform scanned, focused ultrasound hyperthermia treatments of brain tumors," Med. Phys. **14**(2), 228–234 (1987).
[3] M. Tanter, J.-L. Thomas, and M. A. Fink, "Focusing and steering through absorbing and aberrating layers: Application to ultrasonic propagation through the skull," J. Acoust. Soc. Am. **103**, 2403–2410 (1998).
[4] S. Behrens, K. Spengos, M. Daffertshofer, H. Schroeck, C. E. Dempfle, and M. Hennerici, "Transcranial-ultrasound-improved thrombolysis: Diagnostic vs therapeutic ultrasound," Ultrasound Med. Biol. **27**(12), 1683–1689 (2001).
[5] F. J. Kirkham, T. S. Padayachee, S. Parsons, L. S. Seargeant, and F. R. House, "Transcranial measurement of blood flow velocities in the basal cerebral arteries using pulsed Doppler ultrasound: Velocity as an index of flow," Ultrasound Med. Biol. **12**(1), 15–21 (1986).
[6] W. Wilkening, S. Helbeck, T. Postert, J. Federlein, J. Rose, P. Hoppe, T. Buttner, and H. Ermert, "Brain perfusion imaging using contrast agent specific imaging modes," 1999 IEEE Ultrasonics Symposium 2, 1721–1725 (1999).
[7] M. A. Moehring, B. P. Wilson, and K. W. Beach, "Intracranial bleed monitor," 1999 IEEE Ultrasonics Symposium 2, 1545–1549 (1999).
[8] F. J. Fry, R. C. Eggleton, and R. F. Heimburger, "Transkull visualization of brain using ultrasound: An experimental model study," Proceedings of the Second World Congress on Ultrasonics in Medicine, Rotterdam, **47** 97–103 (1974).
[9] P. L. Carson, T. V. Oughton, W. R. Hendee, and A. S. Ahuja, "Imaging soft tissue through bone with ultrasound transmission tomography by reconstruction," Med. Phys. **4**, 302 (1977).
[10] S. W. Smith, D. J. Phillips, O. T. von Ramm, and F. L. Thurstone, "Some advances in acoustic imaging through the skull," Ultrasonic Tissue Characterization II, 209–218 (1979).
[11] K. A. Dines, F. J. Fry, J. T. Patrick, and R. L. Gilmor, "Computerized ultrasound tomography of the human head: Experimental results," Ultrason. Imaging **3**(4), 342–351 (1981).
[12] J. Ylitalo, J. Koivukangas, and J. Oksman, "Ultrasonic reflection mode computed tomography through a skull bone," IEEE Trans. Biomed. Eng. **37**(11), 1059–1066 (1990).
[13] M. Tanter, J.-L. Thomas, and M. A. Fink, "Time reversal and the inverse filter," J. Acoust. Soc. Am. **108**(1), 223–234 (2000).
[14] G. T. Clement and K. Hynynen, "Micro-receiver guided transcranial beam steering," IEEE Trans. Ultrason. Ferroelectr. Freq. Control **49**(4), 447–453 (2002).
[15] S. W. Smith, G. E. Trahey, and O. T. von Ramm, "Phased array ultrasound

imaging through planar tissue layers,'' Ultrasound Med. Biol. **12**, 229–243 (1986).
[16] G. T. Clement and K. Hynynen, ''A noninvasive method for focusing ultrasound through the human skull,'' Phys. Med. Biol. **47**, 1219–1236 (2002).
[17] M. Hayner and K. Hynynen, ''Numerical analysis of ultrasonic transmission and absorption of oblique plane waves through the human skull,'' J. Acoust. Soc. Am. **110**(6), 3319–3330 (2001).
[18] G. T. Clement, J. Sun, and K. Hynynen, ''The role of internal reflection in transskull phase distortion,'' Ultrasonics **39**(2), 109–113 (2001).
[19] M. C. Junger and D. Feit, ''Applications of the Elementary Acoustic Solutions,'' in *Sound, Structures, and Their Interaction* (Acoustical Society of America, Woodbury, NY, 1993).
[20] G. S. Kino, *Acoustic Waves: Devices, Imaging, and Analog Signal Processing* (Prentice-Hall, Englewood Cliffs, NJ, 1987).
[21] R. S. Thompson, P. Tortoli, and G. K. Aldis, ''Selective transmission of a focused Doppler ultrasound beam through a plastic layer,'' Ultrasound Med. Biol. **26**(8), 1333–1346 (2000).
[22] J. Sun and K. Hynynen, ''The potential of transskull ultrasound therapy and surgery using the maximum available skull surface area,'' J. Acoust. Soc. Am. **105**(4), 2519–2527 (1999).
[23] G. T. Clement and K. Hynynen, ''Forward planar projection through layered media,'' IEEE Trans. Ultrason. Ferroelectr. Freq. Control **50**(12), 1689–1699 (2003).
[24] G. T. Clement and K. Hynynen, ''Field characterization of therapeutic ultrasound phased arrays through forward and backward planar projection,'' J. Acoust. Soc. Am. **108**(1), 441–446 (2000).
[25] J. E. Marsden and A. J. Tromba, *Vector Calculus* (Freeman, New York, 1988).